Fractal dynamics of electric discharges in a thundercloud

D. I. Iudin and V. Y. Trakhtengerts
Institute of Applied Physics, Russian Academy of Science, 46 Ulyanov Street, Nizhny Novgorod 603600, Russia

M. Hayakawa*
The University of Electro-Communications, 1-5-1 Chofugaoka, Chofu, Tokyo 182-8585, Japan
(Received 15 November 2001; revised manuscript received 26 March 2003; published 3 July 2003)

We have investigated the fractal dynamics of intracloud microdischarges responsible for the formation of a so-called drainage system of electric charge transport inside a cloud volume. Microdischarges are related to the nonlinear stage of multiflow instability development, which leads to the generation of a small-scale intracloud electric structure. The latter is modeled by using a two-dimensional lattice of finite-state automata. The results of numerical simulations show that the developed drainage system belongs to the percolation-cluster family. We then point out the parameter region relevant to the proposed model, in which the thundercloud exhibits behavior corresponding to a regime of self-organized criticality. The initial development and statistical properties of dynamic conductive clusters are investigated, and a kinetic equation is introduced, which permits us to find state probabilities of electric cells and to estimate macroscopic parameters of the system.

DOI: 10.1103/PhysRevE.68.016601 PACS number(s): 05.65.+b, 05.45.Df, 92.60.Qx, 64.60.Ak

I. INTRODUCTION

Many systems in nature such as physics, chemistry, biology, and even social sciences reveal some common features in their spatiotemporal dynamics, which are now characterized by a common definition as fractal dynamics. The important class of such systems are nonlinear systems with source and sink of free energy, which are able to generate internal dynamic structures [1–3]. The examples are neuron sets in biology, convective streams in hydrodynamics, and multiflow systems in plasma. These systems demonstrate a self-organizing and self-tuning critical behavior when a system comes to the state with universal management of its internal structures, which does not depend on the peculiarities of its separate elements [4–6].

The thunderstorm cloud (TC) seems to be a bright example of such systems. The source of free energy in a TC is updraft convective flow, which forms multiflow streams consisting of air molecules, light droplets, ice crystals, and heavy hail stones. Interaction of these streams with each other leads to the electrical charging of cloud particles and generation of an electric field [7]. A lightning flash that includes leader progression, return strokes, and microdischarges inside of the small-scale cells supply dissipation and sink of free energy in a TC.

Processes in a TC are very diverse and complicated. A classical cloud to ground lightning discharge includes three stages: preliminary breakdown, leader formation, and return stroke [7,8]. The existing theoretical models of lightning discharges are based on its similarity with a laboratory long spark [9]. It actually relates to the leader formation and return stroke. But there is a very important difference, which concerns a preliminary stage of the discharge. In the case of a laboratory spark, electrical charge is accumulated on a conducting wall(s) of a discharge space and flows down easily into the spark channel. It is not clear what mechanism could provide the electric charge gathering over all intracloud volume (or over its considerable part) to the leader channel. Apparently, a certain important process which supplies this gathering takes place during the preliminary breakdown stage. This stage lasts from tens to hundreds of milliseconds, and consists of numerous (up to 10 000) relatively short (with duration about microseconds) discharges (pulses) grouped in trains of various durations. Radio images retrieved with the help of these pulses reveal a strongly forked intracloud network of microdischarges, resembling the structure of fractal clusters. This stage is just discussed in our paper. We suggest a model, which can supply the electric charge gathering over the entire volume of a cloud and bring this charge to the leader channel. This model is based on a two-scale structure of a TC electric field where there exist electric cells with size $l \sim 10$ m much smaller than the cloud size in addition to the large-scale field. Microdischarges which are observed during a breakdown preliminary stage [7,8,10] can be actually considered as indirect evidence of the existence of such small-scale electric cells. There is the physical background for our model based on the beam-plasma instability in a TC [11–13]. This instability predicts the generation of a short-scale electric structure of sizes $\sim 1-10^2$ m. It is borne in mind that the electrical breakdown model which is considered in the paper differs principally from the famous dielectric breakdown model [14] which is based on the step-by-step solution of the Laplace equation $\Delta U = 0$ (U is electrical potential) with the self-consistent moving boundary between infinitely conducting and neutral parts of air. In our case, the Laplace equation is modified by a background air conductivity and by a current of charged cloud particles. The solution of this modified equation is given (in linear approximation) by relation (7), and it predicts the generation of small-scale electric cells. Thus, an intracloud discharge is developing in the electric field, which is initially strongly inhomogeneous. It is natural to suppose

*FAX: +81-424-43-5783; electronic address: hayakawa@whistler.ee.uec.ac.jp

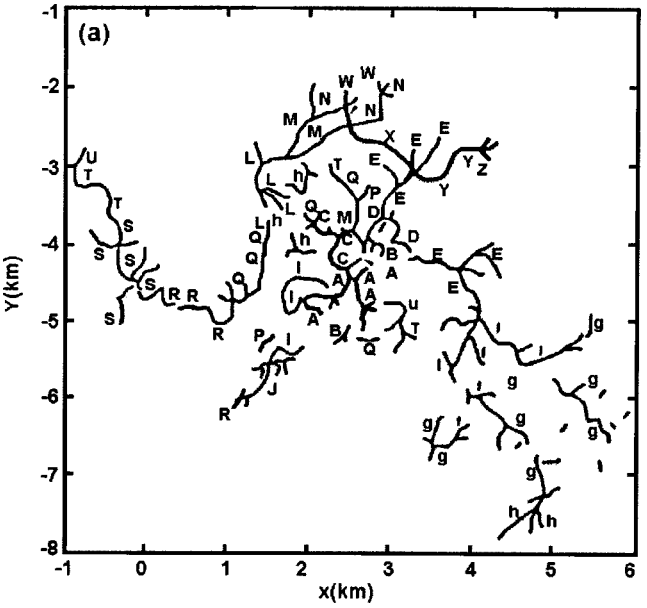

FIG. 1. Plan projection of flash development detected by a VHF mapping system [15]. Letters indicate a sequence of development.

in such a situation that discharges appear inside a separate most intense electric cell and can stimulate discharges in the neighboring cells due to activation processes. In the real atmosphere, such processes can include local inhomogeneities of conductivity or runaway electrons generated by microdischarge inside a neighboring cell. The suitable mathematical model for analyses of cells' interaction is a cellular automation model, which is used below in our computer experiments. We will show below that this system reveals, in a wide range of TC parameters, the features of universal dynamics typical for percolation fractals with self-organized criticality (SOC) behavior. In our case, percolation refers to the process of a TC dynamic metallization on the basis of short-living conducting elements, which appear as a consequence of electrical microdischarges. Such a metallization forms a drainage conducting system, which gathers a macroscopic electric charge over the entire volume of the cloud and determines the development of a macroscopic lightning discharge. There are important experimental evidences of such a scenario, which are seen at the preliminary stage of a lightning flash. Those are multilayer electric field structures that are seen in the *in situ* experiments, and numerous microdischarges on the preliminary stage of lightning flash which are not accompanied by any change in the static electric field. Figure 1 is taken from Proctor [15], which illustrates this microdischarge activity inside a TC.

This paper is organized in the following way. Section II contains a brief description of the features of a TC multiflow instability, which we need for the quantitative formulation of a cellular automation model. This model is described in Sec. III, and some results of the computer experiment are given, which demonstrate the universal behavior of the system. Section IV is devoted to the analysis of the model in the mean-field approach. The kinetic equation is introduced for the potential difference distribution function, which permits us to obtain important mean-field characteristics of the process. In Sec. V, the properties of a dynamic cluster followed from the computer experiment are discussed from the viewpoint of the percolation theory, and we summarize the obtained results in Sec. VI.

II. MULTIFLOW INSTABILITY IN A THUNDERCLOUD

It is well known that a thunderstorm cloud in its mature state consists of different components, which include conducting air, charged heavy particles such as large droplets and hail stones, and charged light particles such as small droplets and ice crystals. The updraft air flow, which is typical for a TC in its mature stage, supplies particle charging and leads to the appearance of a large-scale electric field due to charge separation on the cloud boundaries. The numerical three-dimensional (3D) cloud model was developed (see Refs. [16,17] for details), which permits to obtain the distribution $N_0(\mathbf{r})$ of macroscopic electrical charge over the cloud and value $E_0(\mathbf{r})$ of the macroscopic electric field. A lightning initiation arises in the point, where the magnitude of the electric field is close to the breakdown value. The development of lightning discharge in such a formulation was considered by Mansell, MacGorman, and Straka [18] on the basis of improved dielectric breakdown model (DBM), suggested by Niemeyer, Pietronero, and Wiestmann [14] and Wiesmann and Zeller [19]. This model, however, does not take into account the important peculiarity of a TC, which is connected with a multiflow character of the TC medium. The experience with similar multiflow plasma systems shows that there exists a plasma-beam instability, which leads to the generation of electrostatic waves, drifting together with the flow. Trakhtengerts [11,12] and Mareev, Sorokin, and Trakhtengerts [13] considered this instability as applied to a TC. These waves organize the small-scale electric structure inside a cloud. To illustrate the effect of electric cell generation we consider a simple TC model, which includes two charged components: heavy particles (droplets and hailstones) suspended in the updraft air flow and filling mainly the lower half of the cloud, and the fraction of light particles (air ions, small droplets, and ice crystals) that are carried to the upper part of the cloud.

The initial system of equations includes the equation of motion for charged heavy and light particles,

$$\frac{\partial \mathbf{v}_a}{\partial t}+(\mathbf{v}_a\cdot\boldsymbol{\nabla})\mathbf{v}_a=-(q/M)\boldsymbol{\nabla}U+\mathbf{g}-\mathbf{F}_{fr}/M,$$

$$\frac{\partial \mathbf{v}}{\partial t}+(\mathbf{v}\cdot\boldsymbol{\nabla})\mathbf{v}=-(e/m)\boldsymbol{\nabla}U+\mathbf{g}-\nu_n\mathbf{v}+\mathbf{F}_D/M, \qquad (1)$$

the continuity equations for species, including the continuity equations for the space charge ρ and the electric current $\mathbf{j}$:

$$\frac{\partial \rho}{\partial t}+\operatorname{div}\mathbf{j}=0, \qquad (2)$$

where

$$\rho=en+qN, \quad \mathbf{j}=en\mathbf{v}+qN\mathbf{v}_a, \qquad (3)$$

and the Poisson equation for the electric potential U,

$$\nabla^2 U = -4\pi\rho. \tag{4}$$

In system (1), $\mathbf{v}_a$ is the velocity, q and M are the charge and mass of heavy particles, g is acceleration due to the gravity, and $\mathbf{F}_{fr}$ is the friction force in the updraft air flow; accordingly, $\mathbf{v}$ is the velocity and e and m are the charge and mass of light particles, $\mathbf{F}_D$ is the force creating the updraft air flow. In relation (3), n and N are the densities of light and heavy particles accordingly.

We shall analyze the initial stage of electric cell generation, when variations of the concentration and the velocity of heavy and light particles are small, that is,

$$\tilde{N}/N_0 \ll 1, \quad |\tilde{n}|/n_0 \ll 1, \quad |\tilde{v}|/v_0 \ll 1, \quad |\tilde{v}_a|/v_0 \ll 1, \tag{5}$$

where N_0, n_0 are the stationary concentrations of heavy and light charged particles, which follow, for example, from 3D calculations [16–18], v_0 is updraft velocity, $\tilde{v} = v - v_0$ and $\tilde{v}_a$ are the velocity variations of heavy and light charged particles accordingly. In this approach, from the initial system of equations (1)–(4), we obtain the Poisson equation for the electrical potential with the self-consistent space charge that is not taken into account in the traditional DBM:

$$\left[\frac{\partial}{\partial t} + (\mathbf{v}_0 \cdot \boldsymbol{\nabla}) + 4\pi\sigma\right]\nabla^2 U = 4\pi q\left[\frac{\partial}{\partial t} + (\mathbf{v}_0 \cdot \boldsymbol{\nabla})\right]\tilde{N},$$

$$\frac{\partial}{\partial t}\left(\frac{\partial}{\partial t} + \nu\right)\tilde{N} = (N_0 q/M)\nabla^2 U, \tag{6}$$

where σ is air conductivity (without charged heavy particles), ν is the effective collision frequency that is equal to $\nu = g/v_0$ for suspended particles. If we are interested in spontaneous generation of electric cells with scale much less than the cloud scale, the boundary conditions are not important. In frame of Eq. (6), the electric cell generation manifests itself as the instability that leads to the exponential growth of small variations of U. The wave potential U and the variation $\tilde{N}$ during the linear stage of the instability development can be presented in the form U, $\tilde{N} \sim \exp(-i\omega t + i\mathbf{k}\cdot\mathbf{r})$, where $\mathbf{r}$ and t are the spatial coordinate and time, respectively. Substituting this presentation into Eq. (6), we obtain the following dispersion relation between the wave vector $\mathbf{k}$ of the electric wave and its frequency ω [11,12]:

$$1 - \frac{\Omega^2}{\omega(\omega + i\nu)} + \frac{4\pi i\sigma}{\omega - \mathbf{k}\cdot\mathbf{v}_0} = 0, \tag{7}$$

where $\Omega^2 = 4\pi q^2 \tilde{N}/M$ is the square of the "heavy particle gas" plasma frequency. The instability threshold is given by the condition $(\Omega/\nu)^2 \geqslant 1$ and the instability growth rate is derived as $\gamma \simeq 2\pi\sigma(\Omega/\nu)$ for the optimal spatial period $a \sim \pi/k \simeq \pi v_0/\Omega$. For particle radius ~ 0.5 cm and $N \sim 10^3\ \mathrm{m}^{-3}$, the instability threshold is achieved for $q \sim 10^{-10}$ C. Putting $v_0 \sim 10$ m/s and $\Omega \sim 2\nu$, we find $\nu \sim 1\ \mathrm{s}^{-1}$, $a \sim 10$ m, and $\gamma \sim 4\pi\sigma\ \mathrm{s}^{-1}$. Our further research [13] with taking into account charge exchange between particles has shown this instability to be universal in a wide range of the cloud parameters. At the nonlinear stage, a small-scale electric field amplitude is determined by a balance between the electric force and the force of gravity acting on a large particle: $E \sim Mg/q \sim 10^6$ V/m. Therefore, the amplitude of the small-scale electric field can be much larger than the mean magnitude of a large-scale intracloud field. We assume that the amplitude growth of the small-scale field is limited at some critical value beyond which a spark discharge between the electric-wave maxima and minima is developed. These breakdowns limit the instability development and determine the microdischarge activity on the lightning preliminary stage.

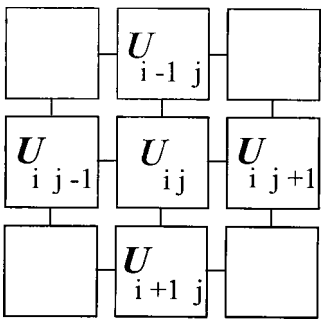

FIG. 2. Square-lattice model. Each site of the lattice is related to a time-dependent electric potential U_{ij}.

III. MODEL

We suggest that the evolution of a small-scale electric structure during the preliminary stage of a lightning discharge is determined by competition between the growth process caused by the beam-instability development and the neutralization process related to the appearance of small-scale breakdowns in the intracloud medium. Below, we analyze the details of this interaction using the modeling based on a finite-automata lattice. For clarity, we simulate the small-scale structure of a cloud by the square-lattice elements (see Fig. 2). The lattice step corresponds to the size of a cell of the small-scale electric structure and amounts to about 10 m. With allowance for the fact that the maximum spatial scale of the system is determined by the size of the active part of the TC, which is about a few kilometers, we find that the linear size of the model lattice should be about a few hundred of the spatial period. Each site of the lattice is related to a time-dependent scalar U_{ij} characterizing the electric potential. In our model, the potential differences between the neighboring sites are growing due to the instability effects, as discussed in the preceding section, but the question is what law describes this growth. The fact of the matter that the scale of a TC is very large in comparison with the cell's scale and the conditions for the instability development could be occasional in different parts of a cloud. This problem is needed in a special consideration, which is beyond the scope of this paper. We consider below the simplest random-growth model, in which random values with a normal distribution are added to the electric potentials U_{ij} at the lattice sites at each step of the model time. In this case, each site,

independently of its neighbors, undergoes Brownian motion in the space of electric-potential values. The potential differences ΔU between the neighboring sites is described by the relation

$$\frac{d(\Delta U)}{dt} = \eta(t), \tag{8}$$

where the stochastic force $\eta(t)$ is a white noise with constant dispersion:

$$\langle \eta(t) \rangle = 0, \quad \langle \eta^2(t) \rangle = D. \tag{9}$$

The brackets in Eqs. (8) and (9) mean the averaging. In this case, the energy of the electric field is growing linearly in time:

$$\langle U^2(t) \rangle = Dt. \tag{10}$$

The potential difference growth is limited by some critical value U_c. As soon as this critical value is reached for any two neighboring sites on the lattice, breakdown between the sites takes place and the lattice bond between the sites becomes a conductor. Its conductivity exponentially disappears for a few model-time steps and corresponding potential difference levels down. We assume that such a fine scale spark discharge can initiate breakdowns of the neighboring lattice bonds (''infect'' the neighbors). It occurs if the potential difference between them exceeds some activation level U_a, which is less than the critical one. Here it is appropriate to mention analogy with the experiments [20] on the laser-beam initiation of a spark discharge, in which the breakdown field is decreased several times under the action of the radiation. After a breakdown, the corresponding lattice bond returns to the deactivated state with zero potential difference.

So, each bond of the lattice can be in one of the three different states: the bond can be an insulator with voltage drop absolute value that is less than the activation level U_a—passive bond; the bond can be an insulator with voltage drop absolute value that exceeds the activation level U_a and is less than the critical value U_c—activated bond; the bond can be a conductor with voltage drop absolute value that exceeds the critical value U_c—metallized bond. The lattice is updated simultaneously according to the following algorithm.

(a) An activated bond becomes a metallized one if at least one of its nearest neighbor sites is metallized.

(b) A metallized bond becomes a passive one in the succeeding model-time step. The corresponding voltage drop goes down to zero.

(c) The potential difference random growth ensures transitions from the activated bonds to metallized ones and between passive and activated bonds. Open boundary conditions are assumed.

Figure 3 shows the typical potential relief realized in the numerical experiment. The behavior of the potential difference on a single-lattice bond of the network as a function of the model time is shown in Fig. 4. The cloud electrification and the growth in the small-scale potential relief determine the slow evolution of the intracloud medium which, in turn,

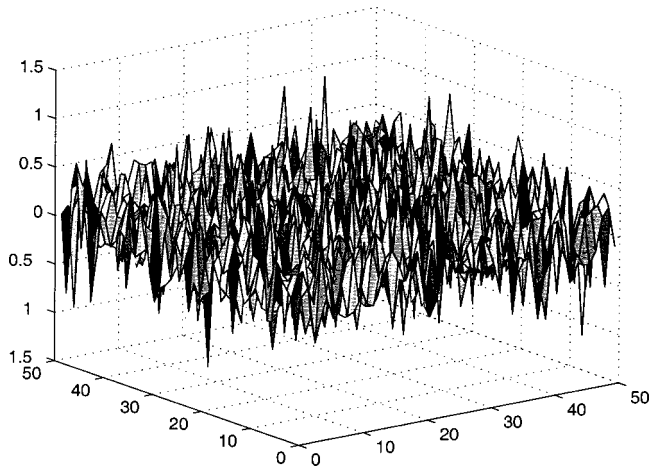

FIG. 3. Potential relief realized on a 50×50 square lattice.

is the background for fast relaxation processes caused by the small-scale discharges. The model parameters are chosen such that a relatively fast dissipation and a slow growth of the potential are ensured. The time step of the automata's life corresponds to the characteristic time of the excitation transfer to its nearest neighbors. In this case, the variation in the potential difference between the neighboring sites during a single step of the model time is smaller than U_c by a few orders of magnitude. Taking into account that the cell size is about 10 m and assuming that the excitation is transferred with a streamer velocity of about 10^7 m/s, we can estimate the model-time step to have a value of about 1 μs. The duration of the preliminary stage of a lightning discharge, lasting from about tens to hundreds of milliseconds, determines the total duration of the model calculation, which therefore should comprise tens to hundreds of thousand of steps.

Let us turn to the results of our numerical experiment. Figure 5 shows the evolution of the specific number of

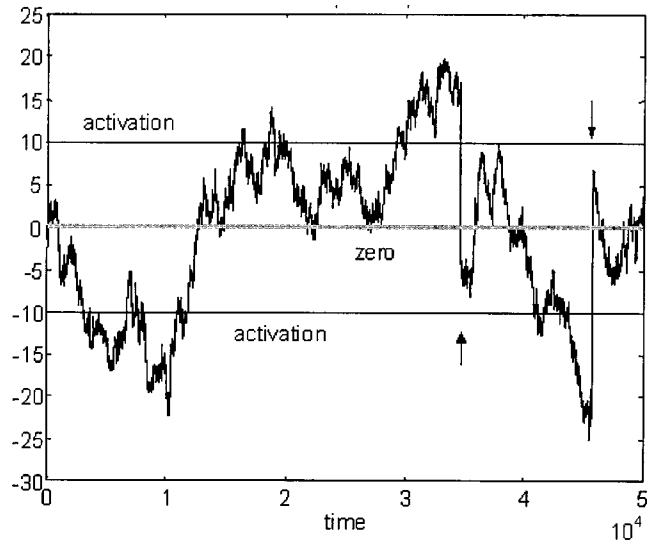

FIG. 4. Time evolution of the potential difference on a single-lattice bond of the network. Arrows indicate the moments when breakdown takes place and the lattice bond becomes a conductor.

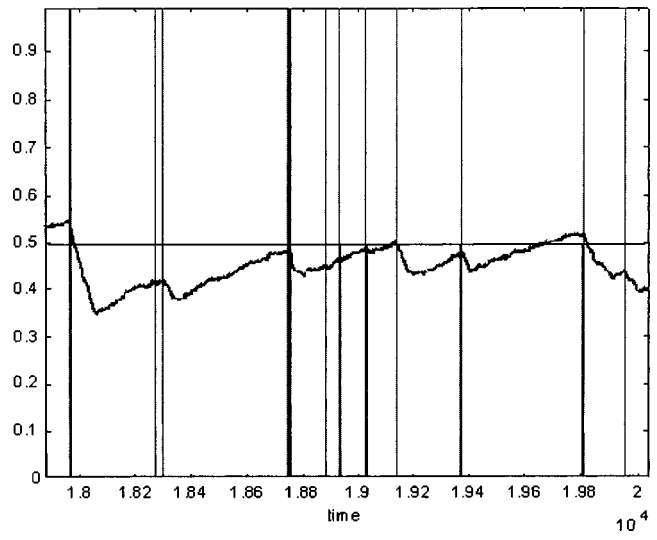

FIG. 5. Time evolution of activated lattice bonds' specific number (heavy line) and evolution of extreme cells' number (δ-shaped splashes of simple length).

activated-lattice bonds. The vertical lines in this figure mark the time instants of the appearance of the critical lattice bonds initiating metallization. It is easy to see that the appearance of critical lattice bonds is an extremely rare event compared to the total number of the small-scale discharges. Moreover, it is seen that the specific value of the activated-lattice bonds fluctuates near the level $p=p_c\simeq 0.5$. This critical level is determined by the combined operation of the external drive (potential relief growth) and the internal relaxation of the threshold dynamics (equalization of the potentials of neighboring cells between which a breakdown occurs). The appearance of new activated-lattice bonds is balanced by their disappearance due to metallization. One can say that the medium is populated by activated elements.

The corresponding temporal evolution of the intracloud-discharge number is presented in Fig. 6. In the case of a low temporal resolution, the events at large times look like δ spikes [see Fig. 6(a)] whose frequency is inversely proportional to the amplitude. On the contrary, if a high temporal resolution is used at short time intervals, the fine structure of individual intracloud discharges can be seen, as determined by the metallization of a distinct cluster of activated-lattice bonds [see Figs. 6(b,c)]. A cluster of activated-lattice bonds is such an aggregate of the activated network elements that any two of these elements can be connected by a continuous chain of the activated-lattice bonds belonging to the aggregate. Of principal importance here is the fact that activated-lattice bond clusters appear to be fractal structures. A snapshot of the process of metallization of an activated-lattice bond cluster is shown in Fig. 7. The white points in this figure correspond to the ionization front, i.e., the local breakdowns during a given step of the model time. The fractal dimension of metallized clusters calculated with allowance for the simulation results is equal to $d_f\simeq 1.9$, which is almost equal to the dimensions of a two-dimensional percolation cluster, as will be seen in Sec. V.

It is not evident that a temporally and spatially homogeneous pumping, i.e., the randomly homogeneous growth of the potential relief, results in the formation of inhomogeneous fractal dissipative structures. Such a clustered dissipation in a cloud is caused by the fact that the inverse growth rate of the small-scale potential relief is a few orders of magnitude greater compared to the time of the excitation transfer from the broken-down element to its nearest neighbors. In this case, even the largest cluster of activated-lattice bonds ''degrades'' faster than the time, when new activated network elements appear among its nearest neighbors. We emphasize the principal importance of such a drastic difference in the time scales in the system considered, which, together with the threshold form of the fast dissipative processes, is generally typical of strong nonequilibrium systems manifesting critical behavior. In Sec. IV, we will see that a big difference in the characteristic time scales characterizing pumping and dissipation is a necessary condition for the spatiotemporal self-similarity of dissipative structures. If this condition is not realized, the system dynamics changes drastically. Indeed, if an activated-lattice bond cluster did not degrade until

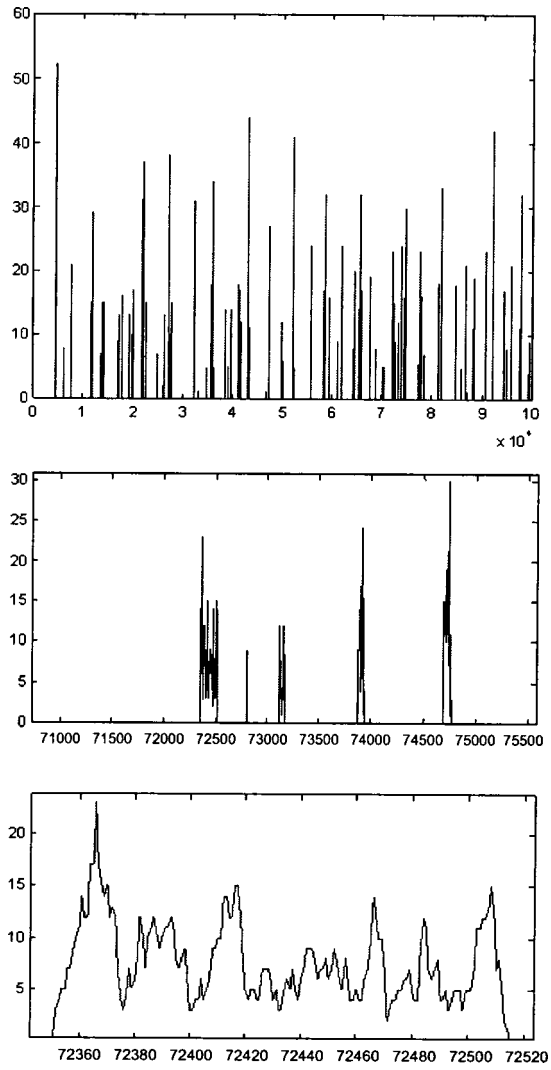

FIG. 6. Intracloud-discharge number temporal evolution. (a)–(c) the scale interval of the horizontal axis varies from 10 000 model time steps in the upper plot to 20 steps in the lower one.

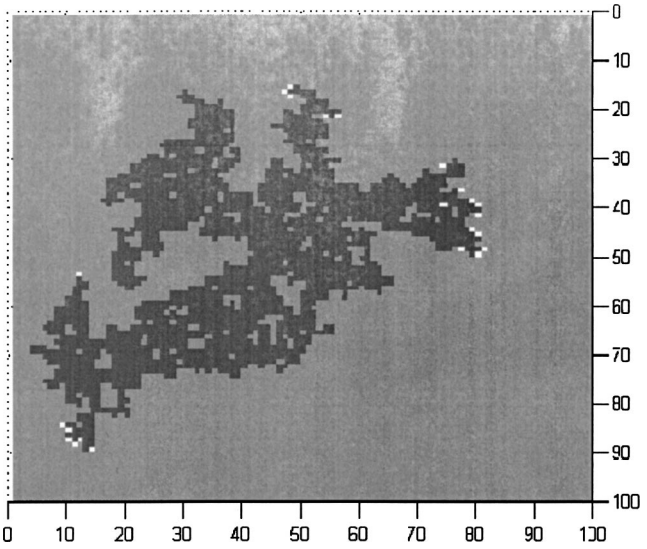

FIG. 7. Metallization process. Gray pixels indicate the area of breakdown spreading; white points correspond to the ionization front.

new activated network elements grew among its nearest neighbors, then the metallization process would never terminate even in the absence of new spontaneous spikes. In this case, repeated ionization fronts of quasiregular spiral form would propagate over the system (see Fig. 8). Note that the characteristic scale of the spirals and the typical distance between them are inversely proportional to the growth rate of the small-scale relief.

To obtain the realizations shown in Figs. 6 and 7, we used a ratio of the activation level U_a to the critical potential difference U_c of about 10% (the value $U_a=0.1U_c$ corresponds to the experimental results on the laser initiation of spark discharge). A smooth increase in U_a/U_c leads to a rapid shrinking of the metallized regions, though their dynamics do not show any serious qualitative changes. However, a decrease of the ratio U_a/U_c at a fixed growth rate of the potential relief leads to disrupting the critical dynamics and establishing the regime of relaxation autooscillations in which the entire network behaves as a single lumped-parameter element. Such a synchronization of the automata is caused by the fact that all these automata overcame the activation level before the first spontaneous breakdown. The reestablishment of the critical dynamics under the fixed U_a/U_c requires an even smaller value of the potential-relief growth rate. Let us turn again to the sequence of metallization spikes shown in Fig. 6 and analyze the statistics of the events. The bilogarithmic plot of the occurrence frequency of metallized clusters comprising N elements as a function of the element number N is presented in Fig. 9. Evidently, this dependence is a power law, which reveals the self-similarity of the space-time dynamics. It is impossible to point out the typical cluster size or typical frequency of their appearance in a wide range of their values. The scaling regime is limited, on the one hand, by the system size and the computing time and, on the other hand, by the size of the one-element clusters and the appearance frequency of such unit clusters. The characteristic time between frequent small events (the appearance of clusters consisting of no more than ten elements) is about a few hundred of model-time steps.

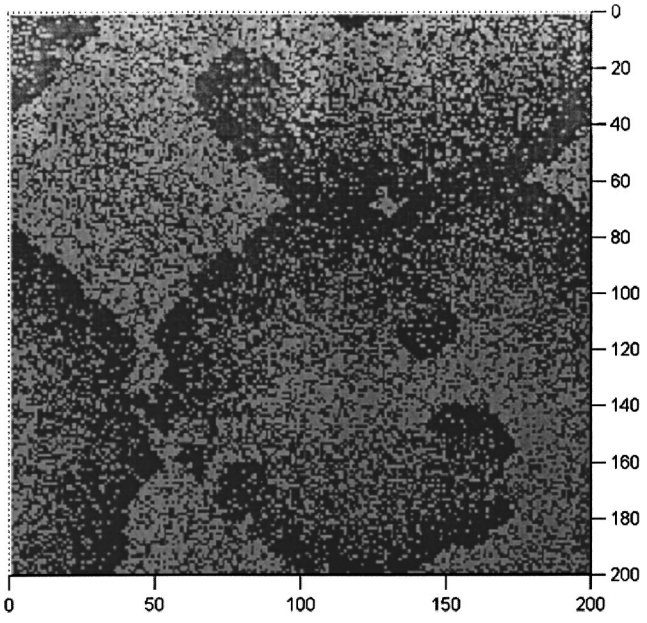

FIG. 8. Formation of quasiregular spiral waves in the network of finite-state automata upon violation of the condition that the time scales of pumping and dissipation are drastically different: snapshot of the system on a 200×200 square lattice.

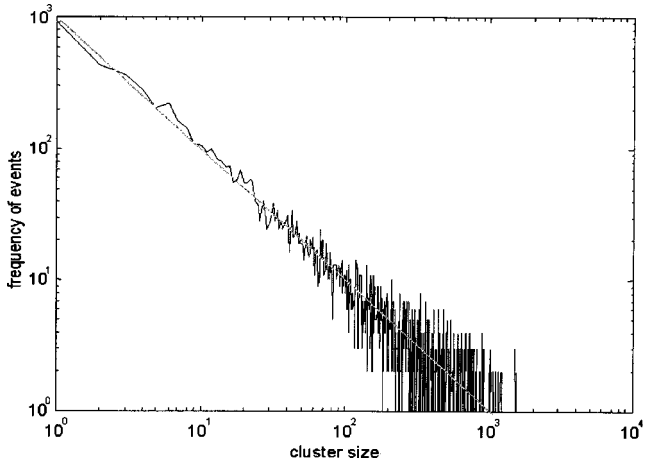

FIG. 9. Occurrence frequency of the metallized clusters as a function of their sizes in log-log scale. The slope of the spectrum is equal to -1.

It is interesting that the scaling properties of the metallization process of a single activated cluster were also observed at a higher resolution at short-term intervals from one to a few hundred of model-time steps. For example, we calculated the average length of the plot $N(t)$, the number of lattice bonds metallized at a specified step, as a function of the averaging interval and find that this value grows faster than a linear function, i.e., $N(t)$ is a fractal of dimension $D_f=1.28$ (see Fig. 10). Using the well-known definition $D_f=2-H$, where H is the Hurst exponent of a generalized Brownian process [6], we arrive at the following asymptotic relation confirmed by the numerical experiment:

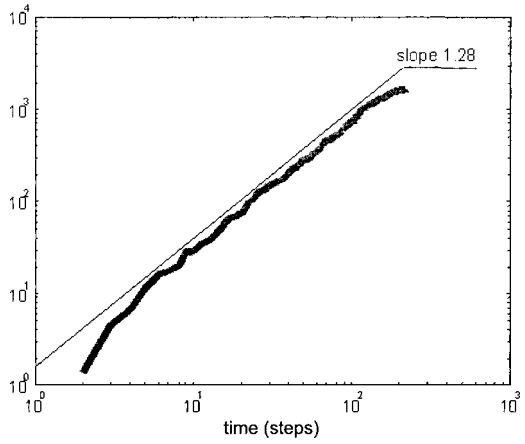

FIG. 10. Dependence of the length of the plot $N(t)$ on the time interval, obtained numerically. The slope of the bilogarithmic plot of the obtained dependence determines the fractal dimension $D_f \simeq 1.28$ of the plot.

$$N(t) \sim t^{0.72}. \tag{11}$$

In Sec. V, we compare obtained results with the regularities which follow from the percolation theory.

IV. MEAN-FIELD APPROXIMATION

In this section, we intend to point out the general criteria for the appearance of critical dynamics. For example, the numerical experiment revealed the existence of a critical population level such that fluctuations near it have scaling properties. Moreover, the experiment revealed the dependence of this level on the number of nearest neighbors for a given automata lattice, i.e., on the lattice coordination number z. The more the elements contact the ''infected'' one, the higher is the probability of the ''infection'' spreading and, therefore, the lower is the critical population level. The coordination number increases with increasing lattice dimension. In the limit of large coordination numbers, the mean-field approach can be applied to calculate the critical population level. The mean-field approach is interesting for the estimation of other mean characteristics of our system such as the number of passive (nonactivated) and critical (metallized) cells as well for the definition of parameters, where the system reveals features of SOC behavior. Let us introduce the distribution function $f(U)$ of lattice bonds over the magnitude of potential difference on them. The quantity $f(U)dU$ determines the fraction of lattice bonds with a potential difference magnitude in the interval from U to $U+dU$, and it is evident that $\int_0^\infty f(U)dU=1$. The specific fraction of the activated-lattice bonds is given by

$$p=\int_{U_a}^{U_c} f(U)dU \tag{12}$$

and plays the role of a specific critical parameter of the system. Taking into account the random-growth model (8)–(10) and the character of neighboring cell's interaction, it is possible to write the kinetic equation for the distribution function f in the form

$$\frac{\partial f}{\partial t}=D\frac{\partial^2 f}{\partial U^2}+I-\nu f, \tag{13}$$

where D is the absolute value of potential difference, and the last two terms on the right hand side characterize the source and the sink, which are equal to

$$I=\begin{cases} \nu_0 m\,\delta(U), & u\leqslant U_a \\ 0, & U_a\leqslant U\leqslant U_c \\ \nu_0 z p f, & U_c\leqslant U \end{cases} \tag{14}$$

and

$$\nu=\begin{cases} 0, & u\leqslant U_a \\ \nu_0 m z, & U_a\leqslant U\leqslant U_c \\ \nu_0, & U_c\leqslant U, \end{cases} \tag{15}$$

where $m=\int_{U_c}^{\infty} f(U)dU$ is the number of metallized bonds, z is the lattice coordination number, $\delta(U)$ is the Dirac delta function, p is determined by Eq. (12), and ν_0^{-1} is the model-time step (duration of a bond breakdown). The three regions of U we use in Eqs. (14) and (15) correspond to the three types of bonds we consider. For example, the term $\nu_0 m z$ in Eq. (15) describes the loss density of activated bonds due to the breakdown spreading from one of the mz neighbor metallized bonds. The number of passive cells is equal to

$$q=\int_0^{U_a} f(U)dU. \tag{16}$$

Because all lattice bonds of the model fall into one of three complementary categories, the densities must add up to unity. That is,

$$p(t)+q(t)+m(t)=1. \tag{17}$$

It is easy to find the stationary solution of Eq. (13) by requiring the continuity of f and $\partial f/\partial t$ and putting $f\to 0$ at $U\to\infty$. Using the dimensionless variable $y=U/U_a$, we obtain

$$f=\begin{cases} m\tau(1-y)+(m\tau/z)^{1/2}(1+a)/(1-a) & \text{if } 0\leqslant y\leqslant 1, \\ \sqrt{m\tau/z}\{\exp[-\sqrt{m\tau z}(y-1)]+a\exp[\sqrt{m\tau z}(y-1)]\}/(1-a) & \text{if } 1\leqslant y\leqslant y_c, \\ 2\sqrt{m\tau/z}\exp[-\sqrt{m\tau z}(y_c-1)]\times\exp[\sqrt{\tau(1-pz)}(y_c-y)]/[(1-a)\sqrt{1+(1-pz/mz)}] & \text{if } y_c\leqslant y\leqslant\infty, \end{cases} \tag{18}$$

where $\tau = U_a^2 \upsilon_0 / D$, $m = \int_{y_c}^{\infty} f\, dy$ is the number of metallized cells, $y_c = U_c / U_a$, and parameter a is equal to

$$a = \frac{\sqrt{mz} - \sqrt{1-pz}}{\sqrt{mz} + \sqrt{1+pz}} \exp[-2\sqrt{m\tau z}(y_c - 1)]. \quad (19)$$

Integrating Eq. (18) we find p,

$$p = \frac{1}{z}\left\{1 - \frac{2\sqrt{1-pz}\,\exp[-\sqrt{m\tau z}(y_c-1)]}{(1-a)(\sqrt{mz}+\sqrt{1-pz})}\right\}. \quad (20)$$

The number of nonactivated cells is determined by the following relation:

$$q \equiv \int_{y_c}^{\infty} f\, dy = m\tau/2 + \frac{1+a}{1-a}\sqrt{m\tau/z}. \quad (21)$$

Relations (20) and (21) together with condition (17) give us the particular values of q, p, m as functions of the parameters z, τ, and y_c. Function (18) together with the analysis of the nonstationary problem of Eq. (13) permits us to investigate all possible solutions which take place for different values of z, t and y_c, including the solutions which were obtained in our computer experiments (Figs. 7 and 8). We restrict ourselves to the analysis of only the case when our system reveals the fractal and self-tuned behavior. As it follows from the computer experiment, such a behavior takes place when $\tau \gg 1$ and $p \gg m$. According to relations (18)–(21), both inequalities are fulfilled under the following condition:

$$\sqrt{m\tau z}(y_c - 1) \gg 1. \quad (22)$$

Just in this case the system reveals SOC dynamics and according to Eq. (20) is determined only by the coordination number

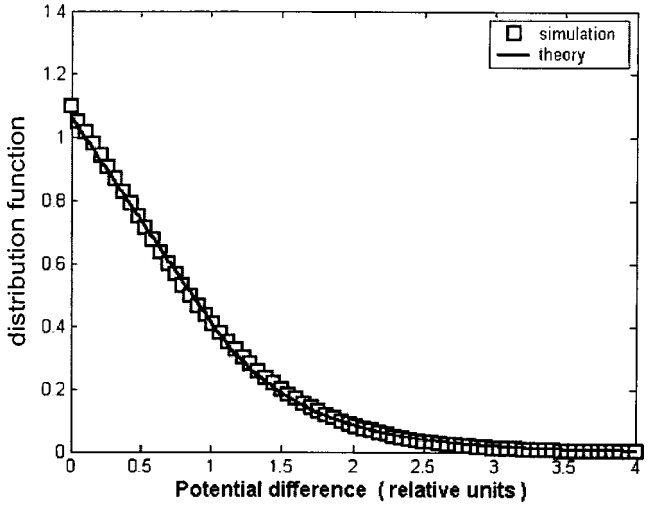

FIG. 11. Comparison between mean-field theory and simulation.

$$p \approx z^{-1}. \quad (23)$$

Relations (17), (21), and (23) give us the value of m:

$$2(z - \sqrt{2z-1})/\tau z. \quad (24)$$

Now inequality (22) can be written in the form

$$\delta \equiv (2z - 2\sqrt{2z-1})^{1/2} \gg \frac{1}{y_c - 1}. \quad (25)$$

In our computer experiments, $z = 3$, $y_c = 10$, and $\delta = 1.2 \gg (y_c - 1)^{-1} = 0.11$, so that inequality (22) is fulfilled. The distribution function (18) in the limit of Eq. (22) is simplified with the exponential accuracy to the following form:

$$f = \begin{cases} \dfrac{\delta}{z}[\delta(1-y) + \delta] & \text{if } 0 \leqslant y \leqslant 1, \\ \dfrac{\delta}{z}\exp[-\delta(y-1)]\{1 + \exp[-2\delta(y_c - y)]\} & \text{if } 1 \leqslant y \leqslant y_c, \\ 2\dfrac{\delta}{z}\exp[-\delta(y_c) - \Delta(y - y_c)] & \text{if } y \geqslant y_c, \end{cases} \quad (26)$$

where $\Delta = 2\frac{\tau}{\delta}\exp[-\delta(y_c - 1)]$. Function (26) is illustrated in Fig. 11 by a thin line for $z = 3$ ($d = 1.2$), $y_c = 10$, and $\tau = 25$. Here the distribution function is shown as well as squares in the figure, which is obtained in the computer experiment for the same values of z, y_c, and $\tau = 25$. One can see a rather good coincidence in the main part of distribution, but the difference grows at the tail of distribution for $y > y_c$. In particular, it follows from the theoretical model (26) that the number of critical cells $m \simeq 2 \times 10^{-2}$; at the same time, the computer experiment gives $m \simeq 10^{-4}$. The reason of such a discrepancy is apparently the same as the mismatch in the values of the critical parameter p_c, which is determined in the mean-field approach by relation (23), $p_c \simeq z^{-1}$, and considerably differs from the computed value, $\langle p \rangle \approx 0.44$, close to the percolation threshold (Fig. 5). This cause is in strong fluctuations of a connection number, which exists in the systems with low values for the coordination parameter z. The similar situation appears in SOC forest-fire models [16]. Indeed, we should take some effective value of $z_{\text{eff}} < z$, which is close to z for $z \gg 1$. In particular, a much

better agreement of the mean-field approach with the computer experiment takes place for $z_{\text{eff}}=1/\langle p\rangle\approx 2.3$. The distribution function for this case is shown in Fig. 11 by a thick line.

V. PERCOLATION STRUCTURE OF METALLIZED CLUSTERS

Now we compare the properties of our dynamical fractal obtained from the computer experiment, with the well-known percolation fractal [6,21,22]. Actually we have three parameters for such a comparison: the averaged number of activated cells p, the fractal dimension d_f of dynamic activated cluster, and the Hurst number H. It is borne in mind that we are dealing with a dynamic fractal, while the percolation is usually considered as a geometrical phase transition. So, let us discuss the percolation process with this point of view. When our system comes to a stationary (on average) state, the clusters are generated in time as a dynamic property of the system. In this case an ensemble of realizations, which is needed to get the averaged characteristics of a fractal, is obtained actually as a temporal consequence. The correct estimation of fractal critical parameters demands a sufficiently long temporal realization. Here the situation reminds ergodic processes, when the average over an ensemble is equal to the average over time. So, we can obtain the critical parameters of our system, using the time averaging, as it has been done in Sec. III. Acting so, we obtained the number of activated cells, which characterizes in our case the phase transition from the dielectric state to the electrically conducting state of a TC medium. According to our computer experiment, this value is equal to $\langle p\rangle\approx 0.44$ (see the realization in Fig. 5), which is close to the percolation threshold $p_c=0.5$ for bonds in a 2D case. Similarly, we found the fractal dimension d_f, using the averaging over the temporal series of activated clusters. It turns out to be equal to the fractal dimension of two-dimensional percolation cluster $d_f^p=1.89$ [6]. The important indication of SOC systems is the power spectrum of occurrence frequency of the clusters as a function of their sizes with the power exponent $\alpha=-1$. The close dependence is revealed in our experiments, as shown in Fig. 9.

To obtain additional information on the structure of a cluster, formed in the course of the metallization, let us remind some properties of a fractal as geometrical object. We consider the shortest path (so-called chemical distance) between two points of the cluster along the cells, belonging to this cluster. According to the fractal theory, the cluster mass M (the number of the cluster's cells) is changing as

$$M(l)\propto l^{d_1}, \tag{27}$$

where l is the chemical distance length, and the chemical dimension $d_l=1.72$ for the percolation cluster. The relation can be rewritten as

$$N(l)\propto dM/dl\propto l^H, \tag{28}$$

where the Hurst exponent $H=0.72$ characterizes our fractal formation as a generalized Brownian process [6]. In our case

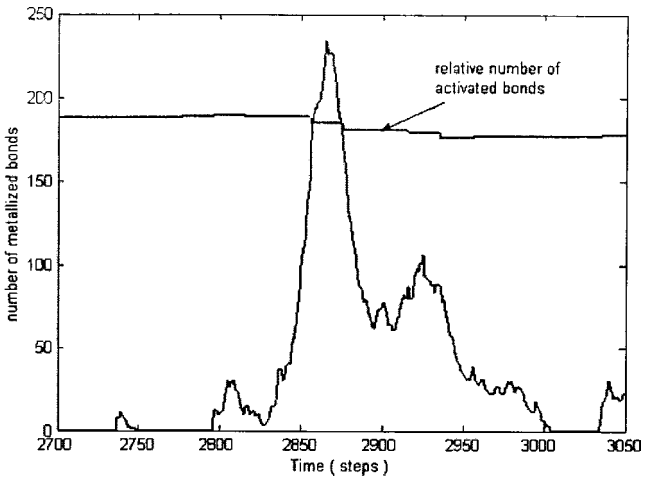

FIG. 12. Temporal growth of the conducted cell number in comparison with the evolution of the activated bond relative number.

$l\sim t$, and we can see that the Hurst exponent in relation (11) coincides with the power exponent in Eq. (28) following from the percolation theory [6,22,23]. So we can agree quite certainly that we are dealing with the percolation dynamic fractal.

VI. THE INITIAL PROBLEM

The important question is the process of switching on of a drainage system, especially in application to a lightning flash. The preliminary stage of a lightning discharge in the form of numerous electrical microdischarges lasts $\tau_p\sim 10-300$ ms [24] up to the appearance of a leader. At the same time, the growth rate of electric cells $\gamma\sim 0.1$ s corresponds to the time scale $\gamma^{-1}\gg\tau_p$. However, it is borne in mind that the preliminary stage in our model is associated with the development of a conducting percolation cluster, which is switched on by explosive manner (similar to the phase transition). Figure 12 demonstrates the temporal growth of conducted cells' number. We can see that a drainage system as a long chain of conducting cells is switched on for a time $\tau_p\ll\gamma^{-1}$. In real situation, one needs to take into account the real value of an ionization front velocity inside a cloud. According to Proctor's data [10], this velocity $v_i\sim 10^2-10^3$ km/s (the velocity of intracloud streamer). For a cloud size $L\sim 10$ km, it gives $\tau_{p\,\min}\sim 10-10^2$ ms. The further behavior of a conducting percolation cluster is determined by a large-scale electric field, but this question is beyond our present consideration.

It is easy to understand the results in Fig. 12, coming from the mean-field approach (Sec. IV). It follows from the continuity condition for the distribution function f under $y=y_c$ that the number of conducting cells is equal to

$$n=-D\left.\frac{\partial f(t)}{\partial y}\right|_{y=y_c}(1-zp)^{-1}. \tag{29}$$

One can see from Eqs. (26) and (29) that when $zp\neq 1$, n is exponentially small, and $n\to\infty$, when $p\sim p_c\sim z^{-1}$. It says about the explosive behavior of $n(t)$.

VII. CONCLUSION

In this paper, we have studied the electric-discharge dynamics inside a TC as a universal approach to the description of nonequilibrium systems with a developed small-scale internal structure. The global behavior of such systems is weakly dependent on the processes inside individual cells and is determined mainly by the regularities of cell interaction. The most important feature of these systems is fractal dynamics with transition to the self-organized criticality state near the percolation threshold. In a general formulation our model reminds the popular forest-fire models, which demonstrate the features of SOC behavior as well [23]. But this similarity is more as outward. In essence, our initial system describes a wide type of distributed nonlinear systems with a hard excitation, when appearance of local excitation decreases sharply the excitation threshold in neighboring cells. A similar situation can be, for example, in the case of unstable plasma systems, when the instability threshold is determined by an electron-ion collision frequency, which decreases with a temperature growth. So, the instability threshold decreases in neighboring cells due to the local heating.

Another point in our consideration is introducing the consideration of a kinetic equation for a cell state probability, which permits us to obtain in a self-consistent approach the mean characteristics of fractal dynamics.

At the same time, we have demonstrated the important physical background for application of the suggested model to the description of electric-discharge dynamics inside a TC. The principal result of our consideration is the agreement that a TC as an electrically conducting medium reaches a percolation threshold and contains in its mature state a majority of dynamical conducting clusters. These clusters form a so-called drainage system for transport and gathering of a macroscopic electrical charge inside a cloud and can serve as a real basis for explanation of the preliminary stage of lightning discharge.

It is possible to point some particular evidences in proof of this announcement. According to Ref. [24], preliminary stage of a lightning flash starts often in form of numerous discharges without any visible dc field change. It corresponds to a high level activity of small-scale discharges in a big volume of a cloud. The experiment [10,24] gives the appearance frequency of these microdischarges about $10^5\ \mathrm{s}^{-1}$. In our model, this frequency is determined in our model by the relationship

$$F \simeq \gamma \frac{V}{a^3} p, \tag{30}$$

where γ describes the growth rate of the electric field in a cell, V is the volume of the active part of the TC, in which a instability is developed, and p is the fraction of the activated cells. During the stage considered, when the activated-cluster length is comparable to the cloud size, $p \sim p_c$, where $p_c = 0.25$ corresponds to the percolation threshold in the three-dimensional case. Assuming $V \sim 10^{10}\ \mathrm{m}^3$, $\gamma \sim 0.1\ \mathrm{s}^{-1}$, and $a \sim 10$ m, we obtain $F \sim 2.5 \times 10^5\ \mathrm{s}^{-1}$, which agrees well with the experiments [7,8,19]. The important question is about the scale a of the electric cells. In Proctor's experiments, the size a corresponds to the scale of elementary discharge. Basing on the achieved spatial resolution [10], it is possible to say that $a < 60$ m. Our investigations of Eq. (7) for the real parameters of TC (charge and size of cloud particles, background conductivity, updraft flow velocity) give $a \sim 1 - 10^2$ m, which is in good qualitative agreement with the experiment [10]. Measurements [8,10] show that separate pulses with duration $\sim 1\ \mu$s are united in groups, which include tens and hundreds of individual microdischarges. Interferometric measurements [10,24] show that these bursts are equivalent to spatial trains that extend up to some kilometers with the velocity $2 \times 10^7 - 2 \times 10^8$ m/s. We can associate these trains with separate clusters which appear in our model. Near the percolation threshold, a cluster length runs up to cloud size. If a microdischarge corresponds to the spark discharge with characteristic length a, we can estimate a tip velocity as $v_t \sim a/\tau \sim 10^7$ m/s, where $\tau \sim 1\ \mu$s is an elementary discharge duration. This estimation is not in contradiction with experiment data. Precise measurements of a fine electric structure in TC with spatial resolution better than 1 m and 3D computer simulations are needed to get more sophisticated quantitative results. We hope our model will stimulate these investigations.

ACKNOWLEDGMENTS

This work was partly supported by the Russian Foundation for Basic Research (Project No. 01-02-17403). D.I.I. is grateful to the University of Electro-Communications for their support, and V.Y.T. is grateful to the Japanese Government for their support through the University of Electro-Communications.

[1] *Spontaneous Formation of Space Time Structures and Criticality*, edited by T. Riste and D. Sherrington (Kluwer, Dordrecht, 1991).

[2] *Nonlinear Waves: A Collection of Papers*, edited by A. V. Gaponov-Grekhov and M. I. Rabinovich (Nauka, Moscow, 1985), in Russian.

[3] L. S. Polak and A. S. Mikhailov, *Self-Organization in Nonequilibrium Physico-Chemical Systems* (Nauka, Moscow, 1983), in Russian.

[4] P. Bak, C. Tang, and K. Wiesenfeld, Phys. Rev. Lett. **59**, 381 (1987).

[5] P. Bak, *How Nature Works* (*The Science of Self-organized Criticality*) (Springer-Verlag, New York, 1996).

[6] E. Feder, *Fractals* (Plenum, New York, 1988).

[7] D. R. MacGorman and W. D. Rust, *The Electrical Nature of Storms* (Oxford University Press, Oxford, 1998).

[8] M. A. Uman, *The Lightning Discharge*, International Geophysical Series Vol. 39 (Academic, New York, 1987).

[9] E. M. Bazelian and Y. P. Raizer, *Spark Discharge* (CRC, Boca Raton, FL, 1997).
[10] R. U. D. E. Proctor and B. M. Meredith, J. Geophys. Res. **93**, 12 683 (1988).
[11] V. Y. Trakhtengerts, Dokl. Akad. Nauk SSSR **308**, 584 (1989).
[12] V. Y. Trakhtengerts, in *Proceedings of ICAE-92*, edited by J. Latham (A. I. Voeikov Main Geophysical Observatory, St. Petersburg, Russia, 1992), p. 416.
[13] E. A. Mareev, A. E. Sorokin, and V. Yu. Trakhtengerts, Fiz. Plazmy **37**, 123 (1999).
[14] L. Niemeyer, L. Pietronero, and H. J. Wiestmann, Phys. Rev. Lett. **52**, 1033 (1984).
[15] D. E. Proctor, J. Geophys. Res. **86**, 4041 (1981).
[16] J. Straka and J. Anderson, J. Atmos. Sci. **50**, 1329 (1993).
[17] R. C. K. Droegemeir and A. Blyth, J. Atmos. Sci. **55**, 3417 (1998).
[18] C. Z. E. R. Mansell, D. R. MacGorman, and J. Straka, J. Geophys. Res. **107**, 10.1029/2000JD000244 (2002).
[19] H. Weismann and H. Zeller, J. Appl. Phys. **60**, 1770 (1986).
[20] D. Wang, Y. Shimada, S. Uchida, E. Fujiwara, Z.-I. Kawasaki, K. Matsuura, Y. Izaka, and C. Yamanaka, *Noise and Chaos in Space and in the Laboratory*, edited by H. Kikuchi (Plenum, New York, 1994), p. 313.
[21] I. M. Sokolov, Usp. Fiz. Nauk **150**, 221 (1986).
[22] A. Bunde and S. Havlin, *Fractals and Disordered Systems* (Springer-Verlag, Berlin, 1996).
[23] S. Clar, B. Drossel, and F. Schwabl, Phys. Rev. E **50**, 1009 (1994).
[24] G. Labanne, P. Richard, and A. Bondiou, *Lightning Electromagnetics*, edited by R. L. Gardner (Hemisphere, New York, 1990).